Geosci. Model Dev. Discuss., 5, 2527–2569, 2012
www.geosci-model-dev-discuss.net/5/2527/2012/
doi:10.5194/gmdd-5-2527-2012
© Author(s) 2012. CC Attribution 3.0 License.

Geoscientific Model Development Discussions

This discussion paper is/has been under review for the journal Geoscientific Model Development (GMD). Please refer to the corresponding final paper in GMD if available.

Setup of the PMIP3 paleoclimate experiments conducted using an Earth System Model, MIROC-ESM

T. Sueyoshi[1], R. Ohgaito[1], A. Yamamoto[2], M. O. Chikamoto[3], T. Hajima[1], H. Okajima[2], M. Yoshimori[2], M. Abe[4], R. O'ishi[2], F. Saito[1], S. Watanabe[1], M. Kawamiya[1], and A. Abe-Ouchi[1,2]

[1]Japan Agency for Marine-Earth Science and Technology, 3173-25, Showa-machi Kanazawa-ku, Yokohama City, 236-0001, Japan
[2]Atmosphere and Ocean Research Institute, 5-1-5, Kashiwanoha, Kashiwa-shi, Chiba 277-8564, Japan
[3]International Pacific Research Center, Pacific Ocean Science and Technology Bldg., 1680 East-West Road, University of Hawaii, Honolulu, Hawaii 96822, USA
[4]National Institute for Environmental Studies, 16-2 Onogawa, Tsukuba-City, Ibaraki, 305-8506, Japan

Received: 27 July 2012 – Accepted: 9 August 2012 – Published: 3 September 2012

Correspondence to: T. Sueyoshi (sue@jamstec.go.jp)

Published by Copernicus Publications on behalf of the European Geosciences Union.



Abstract

The importance of climate model evaluation using paleoclimate simulations for better future climate projections has been recognized by the Intergovernmental Panel on Climate Change. In recent years, Earth System Models (ESMs) were developed to investigate carbon-cycle climate feedback, as well as to project the future climate. Paleoclimate events, especially those associated with the variations in atmospheric CO_2 level or land vegetation, provide suitable benchmarks to evaluate ESMs. Here we present implementations of the paleoclimate experiments proposed by the Coupled Model Intercomparison Project phase 5/Paleoclimate Modelling Intercomparison Project phase 3 (CMIP5/PMIP3) using an Earth System Model, MIROC-ESM. In this paper, experimental settings and procedures of the mid-Holocene, the Last Glacial Maximum, and the Last Millennium experiments are explained. The first two experiments are time slice experiments and the last one is a transient experiment. The complexity of the model requires various steps to correctly configure the experiments. Several basic outputs are also shown.

1 Introduction

For better future climate projection, the value of evaluating of climate models using experiments over different time scales is gaining recognition. As an experimental design, paleoclimate simulations provide unique opportunities to test models. Recent periods that are climatologically quite different to present day conditions are targeted for the Coupled Model Intercomparison Project phase 5 (CMIP5; Taylor et al., 2009)/Paleoclimate Modelling Intercomparison Project phase 3 (PMIP3). Here we describe three paleoclimate experiments using an Earth system model (ESM) MIROC-ESM, which are conducted as a series of experiments for the Intergovernmental Panel on Climate Change 5th Assessment Report (IPCC AR5).

GMDD

5, 2527–2569, 2012



Model simulations using ESMs, which are Atmosphere-Ocean general circulation models (AOGCMs) coupled with biogeochemical components, are now available for paleoclimate simulations. These models allow evaluation of more components compared to the previous AGCM work in PMIP phase 1, or model inter-comparison using AOGCMs in PMIP phase 2. With ESMs, the carbon cycle and biogeochemical processes can be calculated on-line as a model component. As the carbon dioxide plays a crucial role in controlling radiation, ESMs are being increasingly used in global climate change projection.

For IPCC AR5, three paleoclimate experiments were officially listed in the CMIP5/PMIP3 project (Taylor et al., 2009; Otto-Bliesner et al., 2009): exp. 3.4, Mid-Holocene (6000 yr before present time-slice, hereafter 6 ka), exp. 3.5, Last Glacial Maximum (21 000 yr before present time-slice, hereafter LGM) from Tier 1, and exp. 3.6 Last Millennium (850–1850 AD transient, hereafter LM) from Tier 2. We briefly review the type of scientific questions that draw the attention of the paleoclimate community.

The pronounced characteristics in the climate reconstruction during 6 ka are the enhancement of African and Asian summer monsoons and the associated enhanced vegetation activity over the Sahara desert (Hoeltzmann et al., 1998; Jolly et al., 1998; Peyron et al. 2006). The enhancement and northward shift of the summer African and Asian monsoons were reported in PMIP phase 1 (Joussaume et al., 1999) and PMIP phase 2 (Braconnot et al., 2007). These changes were consistent in sign with paleoclimate proxy records, mostly from pollen (Kohfeld and Harrison 2000; Prentice et al., 2000; Yu et al., 2000; Harrison et al., 2001, 2003; Bigelow et al., 2003; Pickett et al., 2004; Bartlein et al., 2010), but most of the models failed to simulate enough precipitation enhancement to maintain a vegetated Sahara (e.g. Doherty et al., 2000; Chikira et al., 2006). Many modeling works have investigated the vegetation feedback effect on the African monsoon change in 6 ka, and most have described the presence of positive feedback between vegetation and precipitation (Ganopolski et al., 1998; Doherty et al., 2000; Levis et al., 2004). Several studies investigated the role of the ocean on the summer monsoons using AOGCMs, and most suggested that there is further enhancement

GMDD
5, 2527–2569, 2012



of the African monsoon when the ocean is coupled, contrasted with attenuation of the Asian monsoon (Liu et al., 2003; Zhao et al., 2005, 2007; Ohgaito and Abe-Ouchi, 2007, 2009; Zhao and Harrison, 2011). Dallmeyer et al. (2010) used an ESM to investigate the effect of the ocean and vegetation component on the total change of the Asian monsoon, and found that the ocean plays a major role in the enhancement of precipitation. Experiments with ESM coupled with dynamic global vegetation models provide an opportunity to evaluate the comprehensive influence on Asian and African monsoon change resulting from dynamic vegetation and oceans.

The LGM was characterized by a very cold and dry climate. The Laurentide and Fennoscandian ice sheets covered North America and Northern Europe (e.g. Denton and Hughes, 1981), atmospheric greenhouse gas (GHG) levels were reduced, and dust transportation was enhanced. (e.g. Barnola et al., 1987; Petit et al., 1981). Land vegetation responded as well: subtropical deserts expanded and forests generally regressed (Colinvaux et al., 1996, 2000; Marchant et al., 2009). At high latitudes, boreal forests migrated southward, replaced by tundra and grassland (Prentice et al., 2000; Tarasov et al., 2000; Ray and Adams, 2001; Harrison and Prentice, 2003). Due to these significant differences from today, various aspects of the climate can be investigated. For example, attempts to constrain climate sensitivity using LGM cooling (Annan et al., 2005; Schmittner et al., 2011), the mechanism of the recorded weakening of the Atlantic Meridional Overturning Circulation (AMOC) and the associated cooling in the North Atlantic Ocean (Weber et al., 2007; Murakami et al., 2008), and southward shift of the Intertropical Convergence Zone (ITCZ) and weakened monsoon activities (Rojas et al. 2009) have been studied. Temperature changes have been discussed in comparison with archives of proxy records (Otto-Bliesner et al., 2009; MARGO project members, 2009; Bartlein et al., 2010). With respect to the carbon cycle, the glacial-interglacial atmospheric CO_2 variations remain an open issue (Kohfeld and Ridgwell, 2009). LGM climate experiments using ESM with an interactive carbon cycle, will contribute to the understanding of the mechanisms controlling CO_2 variations.

GMDD
5, 2527–2569, 2012



The LM includes two key climatic epochs: the "Medieval Climate Anomaly" (MCA, ca. 1000–1200 AD) and the "Little Ice Age" (LIA, ca. 1500–1850 AD), and has relatively rich proxy data compared to earlier times. Comparison of modelled climate with such observed records is useful in verifying the ability of a climate model, and assists the understanding of the mechanisms contributing to the climate variability. More specifically, the need to distinguish anthropogenic climate change from natural climate variability at centennial to millennial time scales is one of the key issues of climatology, addressing the social demand for climate research. LM experiments with fully coupled ESM allow discussion of the evolution of the carbon cycle interacting with the climate variation over the last 1200 yr.

LM simulations appearing in IPCC 4th Assessment Report (2007) were performed mostly by Earth-system Models of Intermediate Complexity (EMICs) (e.g. Gerber et al., 2003; Goosse et al., 2005). On the other hand, recent progress on proxy-based climate reconstruction has slowly revealed the spatial and temporal extent of various climatic epochs (e.g. Trouet et al., 2009; Mann et al., 2009), which allows better comparison between data and GCM simulations. Following some works with coupled models without a carbon cycle (e.g. Gonzáles-Rouco et al., 2003; Ammann et al., 2007; Servonnat et al., 2010), a LM experiment using an ESM has been reported recently (Jungclaus et al., 2010), and this study follows the same direction in evaluating the strength of natural variability using up-to-date forcing reconstructions.

This paper presents the choice of settings for technical aspects of CMIP5/PMIP3 paleoclimate experiments using MIROC-ESM, including model settings, choice of boundary conditions, special treatment for model spin-up, and the initial data preparation. It is not our intention to present scientific results in detail here, and these will be discussed in subsequent papers.

Model and common settings are described in Sect. 2, specific settings for each paleoclimate experiment are described in Sect. 3 together with preliminary results, and concluding remarks follow in Sect. 4.

GMDD
5, 2527–2569, 2012



2 Model and common settings

MIROC-ESM is an ESM developed at the Japan Agency for Marine-Earth Science and Technology in collaboration with the University of Tokyo and the National Institute for Environmental Studies based on a global climate model MIROC (Model for Interdisciplinary Research on Climate) AOGCM (K-1 Model Developers, 2004; Nozawa et al., 2007). An atmospheric general circulation model (MIROC-AGCM, 2010), including an on-line aerosol component (SPRINTARS 5.00), an ocean GCM with sea-ice component (COCO 3.4), and a land surface model (MATSIRO), are interactively coupled in MIROC-ESM, as illustrated in Fig. 1. These atmosphere, ocean, and land surface components, as well as a river routine, are coupled by a flux coupler (K-1 Model Developers, 2004). As an ESM, MIROC-ESM has a newly introduced atmospheric chemistry component (CHASER 4.1) and carbon-cycle components for the land and ocean ecosystems. The carbon cycle is calculated by a marine biogeochemical component coupled with COCO and a terrestrial ecosystem component dealing with dynamic vegetation (SEIB-DGVM) coupled with MATSIRO. Watanabe et al. (2011) gives detailed descriptions of each component and the model's performance against 20th century climate variations.

The atmosphere and land components have a spatial resolution of T42 (equivalent grid interval is approximately 2.8° in latitude and longitude). The atmosphere has 80 vertical layers between the surface and about 0.003 hPa up to the stratosphere (Watanabe et al., 2008a). Due to the limited computational resources, part of the CMIP5 experiments were performed with the full version of MIROC-ESM, while other experiments, including the paleoclimate experiments described in this paper, were performed using a version without the coupled atmospheric chemistry component (CHASER).

The ocean component COCO (CCSR Ocean COmponent model) has a resolution of 1.4° (longitude) by variable 0.56–1.4° (latitude) in the horizontal and 44 levels in the vertical (K-1 Model Developers, 2004; Hasumi, 2000). No flux correction is applied in exchanging heat, water, and momentum flux between the atmosphere and the ocean.

GMDD
5, 2527–2569, 2012



The sea ice is based on a two-category thickness representation, zero-layer thermodynamics (Semtner, 1976), and dynamics with elastic-viscous-plastic rheology (Hunke and Dukowicz, 1997).

The land surface component MATSIRO (Minimal Advanced Treatments of Surface Interaction and RunOff) consists of a single layer canopy, three layers of snow, and six layers of soil to a depth of 14 m (Takata et al., 2003). It is coupled to a river routing model, TRIP (Total Runoff Integrating Pathways) (Oki and Sud, 1998), for calculating river discharge. The aging effect on snow albedo and the effects of dirt in snow have been taken into account (Yang et al., 1997; Aoki et al., 2006). The dirt concentration in snow is calculated from the deposition fluxes of dust and soot calculated in the aerosol module, SPRINTARS (Spectral Radiation-Transport Model for Aerosol Species) (Takemura et al., 2000, 2002, 2005).

MATSIRO is coupled with the terrestrial ecosystem model SEIB-DGVM (Spatially Explicit Individual-Based Dynamic Global Vegetation Model) (Sato et al., 2007; Ise et al., 2009). SEIB-DGVM adopts an individual-based simulation scheme that explicitly captures light competition among trees, avoiding parameterized competition. Land vegetation is classified into 13 plant functional types (PFTs), and each PFT has different ecophysiological parameters and allometry relationships. This results in differential growth patterns and competition among PFTs under the environmental conditions in each grid cell. Leaf Area Index (LAI) is predicted by computing plant physiological processes such as photosynthesis, respiration, growth, and mortality, at daily time steps under the environment internally reproduced by MIROC-ESM. The predicted LAI is then used for calculation of the biogeophysical processes in MATSIRO: the processes for radiation transfer including surface albedo, interception of precipitation, and energy transfer by latent/sensible heat. In the current configuration, MATSIRO considers the dynamic variations in LAI, while the ground surface type in MATSIRO is fixed, not referring the PFT predicted by SEIB-DGVM. Thus, the terrestrial ecosystem in MIROC-ESM affects climate only through the carbon cycle and the LAI feedback.

GMDD
5, 2527–2569, 2012



The oceanic biogeochemical model is based on a simplified ecosystem of nutrient-phytoplankton-zooplankton-detritus (NPZD) ecosystem model (Oschlies, 2001; Oschlies and Garçon, 1999). The model includes two plankton functional groups of phytoplankton and zooplankton, suspended and sinking particulate detritus, four dissolved inorganic components of alkalinity, dissolved inorganic carbon (DIC) and nitrate. A constant Redfield ratio (C / N = 6.625) is used to estimate the carbon and calcium flow. The sea-air CO_2 flux is calculated by multiplying the difference of ocean-atmosphere CO_2 partial pressures by the ocean gas solubility.

The basic settings of the experiments are common with other CMIP5 historical simulations by MIROC-ESM (Watanabe et al., 2011). Among our paleoclimate experiments, 6 ka and LGM are time-slice experiments conducted to obtain an equilibrium state, while LM is a transient experiment to conduct a time-evolving simulation under the reconstructed time series of boundary conditions.

3 Experimental settings

3.1 Pre-industrial control experiment

3.1.1 Experimental setup

The Pre-Industrial control experiment (PI) (exp 3.1 in CMIP5) is firstly described as a counterpart of the following paleoclimate simulations. PI is forced by the climatic conditions at 1850 AD. The greenhouse gas levels (GHGs) are set to 285 ppm CO_2, 0.3 ppm N_2O and 1.7 ppm CH_4 as listed in Table 1. The land index for MATSIRO is shown in Fig. 2a, based on modern vegetation types with less croplands corresponding to the plausible distribution in 1850. The orbital parameters are set to 0.01672 for the eccentricity, 23.45° for the obliquity, and 102.04° for the angular precession.

GMDD
5, 2527–2569, 2012



3.1.2 Spin-up of the PI data

Initial data for PI experiment was prepared in stages. The procedure is shown in Fig. 3a: starting with the version of MIROC-ESM with 20 vertical layers in the atmosphere, a 380-yr integration was performed as an atmosphere-ocean coupled system, followed by a 50-yr integration with an atmosphere with 80 vertical layers. In the course of the spin-up runs, representative states and fluxes in the physical climate and carbon cycle components were monitored: surface air temperatures, radiation fluxes at the top of the atmosphere, strength of the thermohaline circulation, sea-ice extent, soil and vegetation carbon storage, etc. The spin-up run was continued until linear trends in the last 50 yr of these quantities became insignificant. After these spin-up procedures, a 630-yr integration was carried out as the PI experiment. The last 100 yr are used for the analyses in this paper.

3.1.3 Model performance

The climate of the PI experiment is briefly presented. The sea surface temperature (SST) is shown in Fig. 4 in comparison with the World Ocean Atlas Temperature data (WOA, 1998; Levitus et al., 1998). PI simulated reasonable SST distribution. The global averaged SST in PI is slightly cooler than that in the observational data, because the PI experiment is set to pre-industrial times whilst the observational data were obtained during the 20th century.

The distribution of simulated precipitation in comparison with observational data (Xie and Arkin, 1996) for boreal summer (JJAS) and winter (DJF) are shown in Fig. 5. PI simulates a reasonable representation of the ITCZ and precipitation distribution of the monsoon area. The other basic climate variables (not shown) are generally well represented.

Although the climatic trends were thought to be insignificant, a slight warming drift ($0.1\,^{\circ}\mathrm{C\,century}^{-1}$ in global average surface air temperature) still existed in the PI experiment, which was overlooked during the spin-up procedure. It is considered to be

GMDD
5, 2527–2569, 2012



due to the slow reduction in sea-ice extent (of 3 % century^{-1}) in the Southern Ocean, which caused a similar warming drift in LM experiment (Sect. 3.4). Because of this drift, additional care is needed in analysis.

3.2 6 ka

3.2.1 Forcing data and boundary conditions

The 6 ka time-slice experiment was performed following the PMIP3 protocol (Table 1). The boundary conditions are kept unchanged from the PI run, except for the orbital parameters (eccentricity: 0.018682, angular precession: 0.87°, obliquity: 24.105°) and GHG concentrations (CO_2: 280.0 ppm, N_2O: 0.65 ppm, CH_4: 0.27 ppm). Volcanic aerosols changes are not considered. Since 6 ka GHG levels are almost the PI condition, this 6 ka condition essentially tests the change in the seasonal incoming shortwave radiation pattern (Fig. 6a) by the orbital parameter settings.

3.2.2 Preparation of the initial data

Figure 3b shows the procedure to prepare the initial data for the 6 ka experiment. We have made a "branch" for 6 ka, deviated from the 250th year in PI with replacing GHG levels and the orbital parameters.

As the land surface condition in the PI experiment includes impacts from anthropogenic land use changes, in 6 ka we initialized the terrestrial ecosystem to a steady state without anthropogenic land usages. To shorten the spin-up time, the initialization was conducted with the off-line terrestrial ecosystem model that is used in MIROC-ESM. Firstly, 100 yr of integration was performed using the 6 ka GHG concentrations and orbital forcing using MIROC-ESM, then surface physical quantities obtained in the last 25 yr (i.e. last 25 yr of "6 ka (1850 land use)" in Fig. 3b) were recursively adapted to the off-line model for 2000 simulation years. After this procedure, the quantities of

GMDD
5, 2527–2569, 2012



terrestrial ecosystems were merged back into the initial conditions for MIROC-ESM, followed by a spin-up of 200 simulation years with all components coupled (Fig. 3b).

3.2.3 Results

The results of the 6 ka experiment are also influenced by the warming drift identified in the PI experiment. In order to minimize the effect of drift, the following analyses are based on the anomalies between 6 ka and PI, and the integration time from the point of initialization of 6 ka (i.e. "branch" time) was kept the same for both experiments.

The changes in simulated temperature 6 ka-PI for JJAS and DJF are shown in Fig. 7. Pronounced changes are the warming over most of the boreal continents by 1–3 °C in JJAS in response to the strengthened solar radiation in the boreal summer. The tropical oceans are slightly cooled. This corresponds to the net negative radiation changes over the tropics compared to PI.

The changes in simulated precipitation are shown in Fig. 8. In JJAS, enhanced precipitation over the Sahel and northern India by 1–3 mm day^{-1} and the reduction of precipitation south of these areas in similar magnitude are simulated. These precipitation changes and the circulation changes suggest an enhancement of the African and Asian monsoon. However, whilst these enhanced monsoons are consistent with the proxy records, the amount of enhancement of precipitation over most of the Sahara Desert is not enough to explain the proxy records. In monitoring the daily-predicted PFTs over the Sahara, SEIB-DGVM predicts non-desert vegetation more often than in the PI case, though they are still much less frequent than desert vegetation. The monsoon activities for the boreal summer are investigated in another work (Ohgaito et al., 2012).

The overall cooling for the boreal winter is seen in Fig. 7, as expected from the radiation change. The precipitation change (Fig. 8) in DJF shows a weakening of precipitation over the continents in the Southern Hemisphere by 0–2 mm day^{-1}, which suggests the weakening of monsoon activities.

GMDD
5, 2527–2569, 2012



3.3 LGM

3.3.1 Forcing data and boundary conditions

The LGM experiment is an equilibrium experiment using the boundary conditions defined by the PMIP3 protocol (Table 1), except the salinity setting. The ocean salinity was assumed to be unchanged from the PI condition.

Atmospheric CO_2/N_2O/CH_4 concentrations, as well as orbital parameters are set to the values shown in Table 1. The shortwave solar radiation deviation at the top of the atmosphere shown in Fig. 6b is much smaller compared to the 6 ka orbital change.

Another major difference in the LGM boundary condition is the topography. The Laurentide and Fennoscandian ice sheets covered wide areas of North America and the northern half of Europe. In the ESM, ice sheets are expressed as mountain ranges with albedo of ice (i.e. flow is not considered). Three ice-sheet reconstructions are currently available: ICE-6G (Peltier, 2009; Argus and Peltier, 2009; Peltier and Drummond, 2008), ANU Ice Model (Lambeck and Chappell, 2001; Lambeck et al., 2002; Lambeck et al., 2003), and GLAC-1 (Tarasov and Peltier, 2002, 2003). Since those reconstructions vary in topography, the settings of our experiment follow the "PMIP standard ice sheet" recommended by the PMIP3 committee, which averages the three reconstructions (PMIP3, 2010). The horizontal resolution of the data provided in PMIP3 ($1^\circ \times 1^\circ$) was regridded to T42 resolution and to the spectral wave number space as other boundary data. The orographic difference for LGM-PI is shown in Fig. 9.

Sea level was lowered by about 90 m, which closes the Bering Strait, and joins together the Indonesian maritime continent. The total mass of the atmosphere was not adjusted. The vegetation boundary condition of the LGM simulation for MATSIRO was created based on the PI vegetation distribution. At first, the vegetation types in the ice sheet area given by the PMIP3 protocol are changed to ice sheet, and the rest of the land areas are basically not changed from PI. However, due to the lower sea level in the glacial climate, the area of the continental shelves should have some vegetation type specified, and the same vegetation types are given as the surrounding grids (Fig. 2).

GMDD
5, 2527–2569, 2012



3.3.2 Preparation of the initial data

The initial data was prepared following the procedure shown in Fig. 3c. The initial condition of the ocean physical field is inherited from the result of LGM experiments by an earlier version of MIROC, MIROC4m (a bug fixed version of MIROC3.2 (medres)), having the same resolution. This experiment has 1900 yr integration under the PMIP2 LGM condition and is regarded as the equilibrium. Since the PMIP3 LGM condition slightly differs from the PMIP2 condition in the ice sheet topography, a spin-up time for the ocean is necessary.

As the atmospheric initial condition, the 250th year of the PI experiment by MIROC-ESM is used, as is the case for the other two experiments. Since MIROC-ESM has a different vertical coordinate system from previous versions, it is difficult to initialize the model by applying the initial condition of these old versions. We thus newly produced the atmospheric initial condition of LGM by starting with PI conditions and conducted the following spin-up for 150 model years. Since the adjustment time of the atmospheric physical field is considerably shorter than that of the ocean, the atmospheric initial condition does not affect the length of the spin-up.

Meanwhile, special care is needed to start an integration under the new topography, which has the large ice sheets in the Northern Hemisphere. The surface pressure field must be adjusted to the change in surface elevation over the continents. As MIROC-ESM has high vertical resolution in the stratosphere, the model was sensitive to the topography change, generating gravity waves and breaking the Courant–Friedrichs–Lewy condition by generating unrealistic high wind velocities. As recommended in the PMIP3 protocol, integration under the new topography can be achieved through two possible methods: either by gradually changing the surface elevation in order to avoid generating gravity waves, or by adjusting the initial pressure field to the LGM surface elevation. In MIROC-ESM LGM, both options were applied.

Since the atmospheric CO_2 concentration in the LGM experiment needs to be reduced by ca. 100 ppm compared to the PI condition, the carbon budget in the initial

GMDD
5, 2527–2569, 2012



data requires long integration to reach a steady state. After the physical field of ESM (i.e. atmosphere-ocean-land) achieved a quasi-equilibrium state, land and ocean biogeochemical components were run separately in an off-line experiment, using the ESM outputs as the required inputs.

The terrestrial ecosystem was spun-up using the offline land ecosystem model, as in the initialization for the 6 ka experiment. The vegetation and soil variables were calculated for 2000 model years under the physical field of the LGM climatology to obtain a steady state. During this initialization process, the influence of anthropogenic land-use was also eliminated. In addition, the prescribed distribution of the ice sheets was used for the processes that prohibit the establishment of new vegetation and accumulations of soil carbon over the ice sheets.

The spin-up of the oceanic ecosystem was performed in a similar manner. Starting from the PI condition, LGM climatology was given recursively to the off-line model (Chikamoto et al., 2012) as boundary conditions for 3500 model years. The partial pressure of the atmospheric CO_2 was set to 185 ppm, to calculate air-sea CO_2 gas exchange. This setting forces the near-surface oceanic pCO_2 to be 189 ppm and achieved a new equilibrium of marine carbon distribution. It results in the removal of the oceanic CO_2, which is equivalent to an increase of ca. 550 ppm CO_2 in the atmosphere.

After these offline experiments had achieved equilibrium, variables are merged back into the experiment using MIROC-ESM and integrated over 200 yr to obtain an equilibrium state for the whole system under the LGM condition.

3.3.3 Results

The change in simulated mean annual temperature for LGM-PI is shown in Fig. 10. More than 20° cooling over the Laurentide and Fennoscandian ice sheets is seen. The rest of the globe cooled much less. Tropical cooling ranges about 1 to 3°, which is consistent with the proxy records (MARGO Project Members, 2009).

GMDD
5, 2527–2569, 2012



The changes in simulated annual precipitation are presented in Fig. 11. The precipitation was reduced for most of the simulated area, suggesting that a drier climate is associated with the cooling.

Although some proxy records suggest the weakening of the AMOC in LGM (McManus et al., 2004), the LGM experiment simulated ca. 32 Sv, which is about 15 Sv stronger peak value of AMOC than that of PI. However, about half of the modelling studies have had a problem representing the weaker AMOC (Weber et al., 2007). Oka et al. (2012) suggested that slight differences in surface cooling or wind stress forcing could lead to the different response of the AMOC. More sensitivity tests using various forcing conditions are required to understand its behavior.

The response of the carbon cycle and predicted vegetation in SEIB-DGVM are investigated in another work.

3.4 LM

The LM experiment is a transient experiment using time-dependent boundary data, unlike the other experiments described in this paper. In addition, the experiment was carried out as a "CO_2 prognostic" run, so that the atmospheric CO_2 concentration was calculated by the model itself. It requires the additional procedure in preparing initial data in terms of atmospheric CO_2 concentration. In this section, the preparation/selection of these data is described.

3.4.1 Forcing data and boundary conditions

The forcing data and boundary conditions for the LM experiment include: (a) orbital forcing, (b) solar forcing, (c) volcanic forcing, (d) non-CO_2 GHGs, and (e) anthropogenic land use.

Orbital forcing is based on a provided time series of parameters (Berger, 1978). As for solar forcing, multiple reconstructions of annual total solar irradiance (TSI) are available, and five reconstructions with different coverage periods are recommended in

GMDD
5, 2527–2569, 2012



the PMIP3 protocol (Schmidt et al., 2012). Amongst these, we used Wang et al. (2005) (hereafter, WLS) for 1610–2000 AD and Delaygue and Bard (2010) (hereafter, DB) for 850–1609 AD (Fig. 12b). WLS is based on a spectral reconstruction and on a flux transport model of the open and closed flux using the observed sunspot record as the main input, while DB is based on an Antarctica stack of ^{10}Be records scaled linearly to the modern-to-Maunder Minimum TSI in the WLS reconstructions. The radiation scheme in MIROC-ESM considers 29 spectral bands, in which spectrally-resolved data provided by WLS can be used directly. The TSI data provided by DB is distributed consistently so that the integrated TSI over the spectra agrees with the reconstruction. No enhanced variations in the UV region proposed by Lean et al. (2000) and used by Shindell et al. (2001) were applied. The parameterization for solar-derived ozone variations suggested by the PMIP3 protocol was not used either.

Two reconstructions of the volcanic forcing: Gao et al. (2008) and Crowley et al. (2008, 2012) are provided by the PMIP3 protocol. Both datasets are based on polar ice cores, but differ in their selection of ice cores, and the Gao data show stronger forcing in general. In our experiment, Crowley data were used (Fig. 12a). The volcanic forcing is calculated using time series of aerosol optical depth (AOD) at 0.55 µm and the effective radius calculated in MIROC-ESM. The data are provided at four latitude bands of equal area. AOD estimates are based on a correlation between sulphate in the Antarctic ice cores and satellite AOD data, which was calibrated with the 1991 eruptions of Mt. Pinatubo and Cerro Hudson (Sato et al., 1993). Aerosol size estimation is based on Pinto et al. (1989).

CO_2, CH_4 and N_2O are considered as GHG forcing in the PMIP3 protocol, and a data table is provided. For the atmospheric CO_2 concentration, however, we decided to perform LM as a prognostic CO_2 experiment in which CO_2 is calculated online (i.e. CO_2 concentration predicted by the carbon cycle component is used for radiation transfer calculation). Thus the model predicts CO_2 using emission data. Anthropogenic emissions are considered only after 1850 AD, while emissions are assumed to be zero for the 850–1850 AD period. CH_4 and N_2O are given as per the PMIP3 data table.

GMDD
5, 2527–2569, 2012



As a difference from the PMIP3 protocol, the anthropogenic land use was assumed to be unchanged. The 1850 condition was applied throughout the experiment including the spin-up period.

3.4.2 Preparation of initial data

As is the case with the 6 ka experiment, pre-industrial physical fields (i.e. from PI experiment) of the atmosphere and ocean were used for the initial data of LM spin-up. Since the forcing conditions: orbital parameters, solar irradiance and GHG concentrations, are quite similar between the pre-industrial period and 800s, PI can be regarded as a spin-up for the 850 AD condition.

Figure 3d shows the procedure of the spin-up. The 250th year of the PI experiment was used as the initial state, then 56 yr of integration was completed under the year-850 condition, with fixed GHG (including CO_2) concentration. Then CO_2 concentration was set to be free, so that the model-calculated value is used in the radiation process of the atmosphere component. At the same time, CO_2 concentration was reset from 298.71 ppm to the level of 279.3 ppm (i.e. value at year 850; Joos, 2007), then the transient simulation was started. This resetting procedure was performed to maintain consistency with the reconstructed value, and also to avoid unnecessary CO_2 feedback. It breaks the conservation of the total carbon in a precise sense, but the effect is small enough to neglect in evaluating the total budget.

3.4.3 Results and time series

Figure 12 shows the time series of (a) volcanic and (b) solar forcing data, (c) the anomaly of simulated annual mean surface air temperature in Northern Hemisphere, and (d) the simulated atmospheric CO_2. Panel (e) shows the same temperature time series as (c), but with the linear trend of warming drift observed in the PI experiment removed (0.094°/100 yr). The blue shade in (e) represents the range of temperature reconstruction between the 20th and 80th percentile by Frank et al. (2010). The air

GMDD
5, 2527–2569, 2012



temperature represents anomalies (°C) from the 1961 to 1990 mean, and is averaged over the Northern Hemisphere for the comparison with proxy records.

The warming drift is clear, especially during the period until the 19th century, while anthropogenic warming is more pronounced during the 20th century. The drift is also visible in the PI experiment, which is caused by a decreasing trend in the Southern Ocean sea ice. It is likely due to an insufficiency of the initialization. Removing the trend is thus necessary to discuss the long-term climate variations; the time series of temperature in panel (e) is obtained by subtracting the linear trend from (c), the slope of which was calculated from linear regression of the PI experiment results for the period between year 250 to year 630 (i.e. after the "branching").

Considering that the proxy data have low-pass characteristics, the time series of the simulated temperature roughly follows the reconstructions for most of the period. However, contrary to the good agreement after the year 1700, some discrepancies can be seen in the earlier periods. For example, the simulated values do not show a clear indication of the LIA, while the reconstruction shows relatively low temperature trends in the 16th to 17th centuries. The mismatch is also large during the 12th century, where the simulated temperature tends to be higher than the reconstruction. The model also seems to overestimate the responses to the huge volcanic events (e.g. year 1229, 1258, 1809, 1816), but this could be due to the limitation of detection capability of the reconstruction method (Mann et al., 2012).

Comparing the simulated temperature anomaly with the forcing data (panel a and b in Fig. 14), it is clear that volcanic aerosols have strong control on the surface air temperature, while the solar irradiance, though visible, has minor effects. Under the current set-up of the model, LM climate variations should depend mainly on those two types of forcing. The faint LIA is considered to be due to the relatively "flat" solar forcing.

The simulated atmospheric CO_2 concentration (panel d in Fig. 12) is stable in the model over the pre-industrial period, while it shows a sharp increase after 1850, the period during which anthropogenic emissions are considered. It shows 399–400 ppm near the surface in the year 2001, while the observed value in Mauna Loa was 370.13 ppm

GMDD
5, 2527–2569, 2012



(Tans and Keeling, 2011) in the same year. Considering that the simulated value at year 1850 was 289.5 ppm, which is ca. 5 ppm higher than the reconstruction, the model still shows a tendency of slight overestimation. This is partly attributable to the warming drift of the global temperature.

4 Conclusions and outlook

The three paleoclimate experiments, 6 ka, LGM, and LM, proposed in CMIP5/PMIP3 were performed using MIROC-ESM. Overall, MIROC-ESM gave qualitatively reasonable results for all three cases. Special care was required when conducting experiments with conditions significantly different from modern simulations, especially using a highly complex model like ESM.

The 6 ka experiment was relatively simple, requiring spin-up only for the land carbon cycle. The results showed reasonable seasonal changes in the temperature distribution in response to the insolation change. The precipitation and the circulation changes suggest the enhancement of the summer African and Asian monsoons. These changes are consistent in sign with the paleo-environmental proxy records, but the enhancement over the Sahara Desert was not large enough, as also seen in previous modelling studies.

The LGM experiment required several steps before starting the simulation. Large change in topography requires a careful adjustment to avoid the numerical instabilities by gravity waves, and very long integration for spin-up is required for the ocean physical state and carbon-cycle variables. In this experiment, ocean values are taken from a LGM experiment using the previous version of MIROC AOGCM, and the spin-up for the carbon cycle was performed separately. In the results, changes in temperature and precipitation are mostly consistent with the SSTs and the pollen proxy records (MARGO Project Members, 2009; Bartlein et al., 2010). AMOC was stronger, which is contrary to the results from some reconstructions. This discrepancy is an issue for many climate models, which should be discussed in another study.

GMDD
5, 2527–2569, 2012



In the LM experiment, the same settings as the PI experiment were used for the fixed boundary conditions. As it is a transient experiment, preparations for time-dependent forcing data are required. Since the experiment was performed as "CO_2 prognostic", the time series of carbon emission data and initialization of the atmospheric CO_2 are also required. After the removal of the linear-regressed temperature trend, the result shows general agreement with the reconstructed hemispheric temperature variations. Since this experiment depends on solar- and volcanic forcing data, updating and cross checking of the data, both for the forcing and proxy records, are continuously required.

It is again recognized that careful and sufficiently long spin-up is mandatory to achieve an equilibrium state, especially for a long transient simulation as LM. In ESMs, more processes such in land and ocean biogeochemistry are considered, and time constants are different among them. In addition to the physical model part, initialization of carbon cycle part is also necessary.

In this paper, we have documented the implementation of the CMIP5/PMIP3 experimental protocol for paleoclimate simulations in MIROC-ESM, with some overview of the results. We have successfully performed the experiments as described here and the results are available via the CMIP5 database (Taylor et al., 2012). Further analysis of each setting, as well as multi-model ensemble analysis will follow this paper. We hope these results contribute to the CMIP5 modelling activity.

Acknowledgements. This study was supported by the Innovative Program of Climate Change Projection for the 21st century, MEXT, Japan. The numerical simulations in this study were performed using the Earth Simulator, and figures were drawn using GTOOL, GrADS, and R. NODC_WOA98 (World Ocean Atlas 1998) data were provided by the NOAA/OAR/ESRL PSD, Boulder, Colorado, USA, from their Web site at http://www.esrl.noaa.gov/psd/. This study is supported in part by the Funding Program for Next Generation World-Leading Researchers by the Cabinet Office, Government of Japan (GR079), by the Green Network of Excellence Arctic Climate Change Research Project, MEXT, Japan, and by the Global Environment Research Fund (S-10) of the Japanese Ministry of the Environment.

GMDD
5, 2527–2569, 2012



References

Aoki, T., Motoyoshi, H., Kodama, Y., Yasunari, T. J., Sugiura, K., and Kobayashi, H.: Atmospheric Aerosol Deposition on Snow Surfaces and Its Effect on Albedo, SOLA, 2, 13–16, doi:10.2151/sola.2006-004, 2006.

Ammann, C. M., Joos, F., Schimel, D. S., Otto-Bliesner, B. L., and Tomas, R. A.: Solar influence on climate during the past millennium: Results from transient simulations with the NCAR Climate System Model, Proc. Natl. Acad. Sci. USA, 104, 3713–3718, 2007.

Annan, J. D., Hargreaves, J. C., Ohgaito, R., and Emori, S.: Efficiently Constraining Climate Sensitivity with Ensembles of Paleoclimate Simulations, SOLA, 1, 181–184, doi:10.2151/sola.2005-047, 2005.

Argus, D. F. and Peltier, W. R.: Constraining models of postglacial rebound using space geodesy: a detailed assessment of model ICE-5G (VM2) and its relatives, Geophys. J. Int., 181, 697–723, doi:10.1111/j.1365-246X.2010.04562.x, 2010.

Barnola, J. M., Raynaud, D., Korotkevich, Y. S., and Lorius, C.: Vostok ice core provides 160,000-year record of atmospheric CO_2, Nature, 329, 408–414, 1987.

Bartlein, P. J., Harrison, S. P., Brewer, S., Connor, S., Davis, B. a. S., Gajewski, K., Guiot, J., Harrison-Prentice, T. I., Henderson, A., Peyron, O., Prentice, I. C., Scholze, M., Seppä, H., Shuman, B., Sugita, S., Thompson, R. S., Viau, A. E., Williams, J., and Wu, H.: Pollen-based continental climate reconstructions at 6 and 21 ka: a global synthesis, Clim. Dynam., 37, 775–802, doi:10.1007/s00382-010-0904-1, 2010.

Berger, A. L.: Long-term variations of daily insolation and Quaternary climatic changes, J. Atmos. Sci., 35, 2362–2367, doi:10.1175/1520-0469(1978)035<2362:LTVODI>2.0.CO;2, 1978.

Bigelow, N. H.: Climate change and Arctic ecosystems: 1. Vegetation changes north of 55°N between the last glacial maximum, mid-Holocene, and present, J. Geophys. Res., 108, doi:10.1029/2002JD002558, 2003.

Braconnot, P., Otto-Bliesner, B., Harrison, S., Joussaume, S., Peterchmitt, J.-Y., Abe-Ouchi, A., Crucifix, M., Driesschaert, E., Fichefet, Th., Hewitt, C. D., Kageyama, M., Kitoh, A., Laîné, A., Loutre, M.-F., Marti, O., Merkel, U., Ramstein, G., Valdes, P., Weber, S. L., Yu, Y., and Zhao, Y.: Results of PMIP2 coupled simulations of the Mid-Holocene and Last Glacial Maximum – Part 1: experiments and large-scale features, Clim. Past, 3, 261–277, doi:10.5194/cp-3-261-2007, 2007.

GMDD
5, 2527–2569, 2012



Chikamoto, M. O., Abe-Ouchi, A., Oka, A., Ohgaito, R., and Timmermann, A.: Quantifying the ocean's role in glacial CO_2 reductions, Clim. Past, 8, 545–563, doi:10.5194/cp-8-545-2012, 2012.

Chikira, M., Abe-Ouchi, A., and Sumi, A.: General circulation model study on the green Sahara during the mid-Holocene: An impact of convection originating above boundary layer, J. Geophys. Res., 111, D21103, doi:10.1029/2005JD006398, 2006.

Colinvaux, P., De Oliveira, P., Moreno, J., Miller, M., and Bush, M.: A long pollen record from lowland Amazonia: Forest and cooling in glacial times, Science, 274, 85–88, 1996.

Colinvaux, P., De Oliveira, P., and Bush, M.: Amazonian and neotropical plant communities on glacial time-scales: The failure of the aridity and refuge hypotheses, Quaternary Sci. Rev., 19, 141–169, 2000.

Crowley, T. J. and Unterman, M. B.: Technical details concerning development of a 1200-yr proxy index for global volcanism, Earth Syst. Sci. Data Discuss., 5, 1–28, doi:10.5194/essdd-5-1-2012, 2012.

Crowley, T. J., Zielinski, G., Vinther, B., Udisti, R., Kreutz, K., Cole-Dai, J., and Castellano, E.: Volcanism and the little ice age, PAGES news, 16, 22–23, 2008.

Dallmeyer, A., Claussen, M., and Otto, J.: Contribution of oceanic and vegetation feedbacks to Holocene climate change in monsoonal Asia, Clim. Past, 6, 195–218, doi:10.5194/cp-6-195-2010, 2010.

Delaygue, G. and Bard, E.: An Antarctic view of Beryllium-10 and solar activity for the past millennium, Clim. Dynam., 36, 2201–2218, doi:10.1007/s00382-010-0795-1, 2010.

Denton, G. H. and Hughes, T. J.: The Last Great Ice Sheets, Wiley Interscience, New York, 484 pp. and map portfolio, 1981.

Doherty, R., Kutzbach, J., Foley, J., and Pollard, D.: Fully coupled climate/dynamical vegetation model simulations over Northern Africa during the mid-Holocene, Clim. Dynam., 16, 561–573, doi:10.1007/s003820000065, 2000.

Frank, D. C., Esper, J., Raible, C. C., Büntgen, U., Trouet, V., Stocker, B., and Joos, F.: Ensemble reconstruction constraints on the global carbon cycle sensitivity to climate., Nature, 463, 527–30, doi:10.1038/nature08769, 2010.

Ganopolski, A., Kubatzki, C., Claussen, M., Brovkin, V., and Petoukhov, V.: The influence of vegetation-atmosphere-ocean interaction on climate during the mid-Holocene, Science, 280, 1916–1919, doi:10.1126/science.280.5371.1916, 1998.

GMDD

5, 2527–2569, 2012



Gao, C., Robock, A., and Ammann, C.: Volcanic forcing of climate over the past 1500 years: An improved ice core-based index for climate models, J. Geophys. Res., 113, 1–15, doi:10.1029/2008JD010239, 2008.

Gerber, S., Joos, F., Brugger, P., Stocker, T., Mann, M., Sitch, S., and Scholze, M.: Constraining temperature variations over the last millennium by comparing simulated and observed atmospheric CO_2, Clim. Dynam., 20, 281–299, doi:10.1007/s00382-002-0270-8, 2003.

González-Rouco, F.: Deep soil temperature as proxy for surface air-temperature in a coupled model simulation of the last thousand years, Geophys. Res. Lett., 30, 1–4, doi:10.1029/2003GL018264, 2003.

Goosse, H.: Modelling the climate of the last millennium: What causes the differences between simulations?, Geophys. Res. Lett., 32, 2–5, doi:10.1029/2005GL022368, 2005.

Harrison, S. P. and Prentice, C. I.: Climate and CO_2 controls on global vegetation distribution at the last glacial maximum: analysis based on palaeovegetation data, biome modelling and palaeoclimate simulations, Glob. Change Biol., 9, 983–1004, doi:10.1046/j.1365-2486.2003.00640.x, 2003.

Harrison, S. P., Yu, G., Takahara, H., and Prentice, I. C.: Palaeovegetation, Diversity of temperate plants in east Asia., Nature, 413, 129–130, 2001.

Harrison, S., Kutzbach, J., Liu, Z., and Bartlein, P.: Mid-Holocene climates of the Americas?: a dynamical response to changed seasonality, Clim. Dynam., 20, 663–688, doi:10.1007/s00382-002-0300-6, 2003.

Hasumi, H.: CCSR Ocean Component Model (COCO) Version 2.1, CCSR Report, 13, 68 pp., 2000.

Hoelzmann, P., Jolly, D., Harrison, S. P., Laarif, F., Bonnefille, R., and Pachur, H.-J.: Mid-Holocene land-surface conditions in northern Africa and the Arabian Peninsula: A data set for the analysis of biogeophysical feedbacks in the climate system, Global Biogeochem. Cy., 12, 35, doi:10.1029/97GB02733, 1998.

Hunke, E. C. and Dukowicz, J. K.: An Elastic–Viscous–Plastic Model for Sea Ice Dynamics, J. Phys. Oceanogr., 27, 1849–1867, doi:10.1175/1520-0485(1997)027<1849:AEVPMF>2.0.CO;2, 1997.

K-1 model developers: K-1 Coupled GCM (MIROC) Description, K-1 Technical Report No. 1, Center for Climate System Research (Univ. of Tokyo), National Institute for Environmental Studies, and Frontier Research Center for Global Change, available at: http://www.ccsr.u-tokyo.ac.jp/kyosei/hasumi/MIROC/tech-repo.pdf (last access: 30 March 2012), 2004.

GMDD

5, 2527–2569, 2012



IPCC Fourth Assessment Report: Climate Change 2007, edited by: Solomon, S., Qin, D., Manning, M., Chen, Z., Marquis, M., Averyt, K. B., Tignor, M., and Miller, H. L., Intergovernmental Panel on Climate Change, 2007.

Ise, T., Hajima, T., Sato, H., and Kato, T.: Simulating the two- way feedback between terrestrial ecosystems and climate: Importance of forest ecological processes on global change, in: Forest Canopies: Forest Production, Ecosystem Health, and Climate Conditions, edited by: Creighton, J. D. and Roney, P. J., NOVA, New York, 111–126, 2009.

Jolly, D., Prentice, I. C., Bonnefille, R., Ballouche, A., Bengo, M., Brenac, P., Buchet, G., Burney, D., Cazet, J.-P., Cheddadi, R., Edorh, T., Elenga, H., Elmoutaki, S., Guiot, J., Laarif, F., Lamb, H., Lezine, A.-M., Maley, J., Mbenza, M., Peyron, O., Reille, M., Reynaud-Farrera, I., Riollet, G., Ritchie, J. C., Roche, E., Scott, L., Ssemmanda, I., Straka, H., Umer, M., Campo, E. V., Vilimumbalo, S., Vincens, A., and Waller, M.: Biome reconstruction from pollen and plant macrofossil data for Africa and the Arabian peninsula at 0 and 6000 years, J. Biogeogr., 25, 1007–1027, doi:10.1046/j.1365-2699.1998.00238.x, 1998.

Joussaume, S., Taylor, K. E., Braconnot, P., Mitchell, J. F. B., Kutzbach, J. E., Harrison, S. P., Prentice, I. C., Broccoli, A. J., Abe-Ouchi, A., Bartlein, P. J., Bonfils, C., Dong, B., Guiot, J., Herterich, K., Hewitt, C. D., Jolly, D., Kim, J. W., Kislov, A., Kitoh, A., Loutre, M. F., Masson, V., McAvaney, B., McFarlane, N., de Noblet, N., Peltier, W. R., Peterschmitt, J. Y., Pollard, D., Rind, D., Royer, J. F., Schlesinger, M. E., Sytkus, J., Thompson, S., Valdes, P., Vettoretti, G., Webb, R. S., and Wyputta, U.: Monsoon changes for 6000 years ago: Results of 18 simulations from the Paleoclimate Modeling Intercomparison Project (PMIP), Geophys. Res. Lett., 26, 859–862, 1999.

Jungclaus, J. H., Lorenz, S. J., Timmreck, C., Reick, C. H., Brovkin, V., Six, K., Segschneider, J., Giorgetta, M. A., Crowley, T. J., Pongratz, J., Krivova, N. A., Vieira, L. E., Solanki, S. K., Klocke, D., Botzet, M., Esch, M., Gayler, V., Haak, H., Raddatz, T. J., Roeckner, E., Schnur, R., Widmann, H., Claussen, M., Stevens, B., and Marotzke, J.: Climate and carbon-cycle variability over the last millennium, Clim. Past, 6, 723–737, doi:10.5194/cp-6-723-2010, 2010.

Kohfeld, K. E. and Harrison, S. P.: How well can we simulate past climates? Evaluating the models using global palaeoenvironmental datasets, Quaternary Sci. Rev., 19, 321–346, doi:10.1016/S0277-3791(99)00068-2, 2000.

GMDD

5, 2527–2569, 2012



Kohfeld, K. E. and Ridgwell, A.: Glacial-interglacial variability in atmospheric CO_2, Surface Ocean-Lower Atmosphere Processes, Geophysical Research Series 37, Washington DC, American Geophysical Union, 251–286, 2009.
Lambeck, K. and Chappell, J.: Sea level change through the last glacial cycle, Science, 292, 679–686, doi:10.1126/science.1059549, 2001.
Lambeck, K. and Yokoyama, Y.: Into and out of the Last Glacial Maximum: sea-level change during Oxygen Isotope Stages 3 and 2, Quaternary Sci. Rev., 21, 343–360, 2002.
Lambeck, K., Purcell, A., Johnston, P., Nakada, M., and Yokoyama, Y.: Water-load definition in the glacio-hydro-isostatic sea-level equation, Quaternary Sci., 22, 309–318, 2003.
Lean, J.: Evolution of the Sun's Spectral Irradiance Since the Maunder Minimum, Geophys. Res. Lett., 27, 2425, doi:10.1029/2000GL000043, 2000.
Levis, S., Bonan, G. B., and Bonfils, C.: Soil feedback drives the mid-Holocene North African monsoon northward in fully coupled CCSM2 simulations with a dynamic vegetation model, Clim. Dynam., 23, 791–802, doi:10.1007/s00382-004-0477-y, 2004.
Levitus, S., Boyer, T. P., Conkright, M. E., O'Brien, T., Antonov, J., Stephens, C., Stathoplos, L., Johnson, D., and Gelfeld, R.: World Ocean Database 1998, vol. 1, Introduction, NOAA Atlas NESDIS 18, US Government Printing Office, Washington, DC, 1998.
Liu, Z., Brady, E., and Lynch-Stieglitz, J.: Global ocean response to orbital forcing in the Holocene, Paleoceanography, 18, 1–20, doi:10.1029/2002PA000819, 2003.
MARGO Project Members: Constraints on the magnitude and patterns of ocean cooling at the Last Glacial Maximum, Nat. Geosci., 2, 127–132, doi:10.1038/ngeo411, 2009.
Mann, M. E., Zhang, Z., Rutherford, S., Bradley, R. S., Hughes, M. K., Shindell, D., Ammann, C. M., Faluvegi, G., and Ni, F.: Global signatures and dynamical origins of the Little Ice Age and Medieval Climate Anomaly, Science, 326, 1256–1260, doi:10.1126/science.1177303, 2009.
Mann, M. E., Fuentes, J. D., and Rutherford, S.: Underestimation of volcanic cooling in tree-ring-based reconstructions of hemispheric temperatures, Nat. Geosci., 5, 202–205, doi:10.1038/ngeo1394, 2012.
Marchant, R., Cleef, A., Harrison, S. P., Hooghiemstra, H., Markgraf, V., van Boxel, J., Ager, T., Almeida, L., Anderson, R., Baied, C., Behling, H., Berrio, J. C., Burbridge, R., Björck, S., Byrne, R., Bush, M., Duivenvoorden, J., Flenley, J., De Oliveira, P., van Geel, B., Graf, K., Gosling, W. D., Harbele, S., van der Hammen, T., Hansen, B., Horn, S., Kuhry, P., Ledru, M.-P., Mayle, F., Leyden, B., Lozano-García, S., Melief, A. M., Moreno, P., Moar, N. T., Prieto, A., van Reenen, G., Salgado-Labouriau, M., Schäbitz, F., Schreve-Brinkman, E. J., and Wille,

GMDD
5, 2527–2569, 2012



M.: Pollen-based biome reconstructions for Latin America at 0, 6000 and 18 000 radiocarbon years ago, Clim. Past, 5, 725–767, doi:10.5194/cp-5-725-2009, 2009.
McManus, J. F., Francois, R., Gherardi, J.-M., Keigwin, L. D., and Brown-Leger, S.: Collapse and rapid resumption of Atlantic meridional circulation linked to deglacial climate changes, Nature, 428, 834–837, 2004.
Murakami, S., Ohgaito, R., Abe-Ouchi, A., Crucifix, M., and Otto-Bliesner, B. L.: Global-Scale Energy and Freshwater Balance in Glacial Climate: A Comparison of Three PMIP2 LGM Simulations, J. Climate, 21, 5008–5033, doi:10.1175/2008JCLI2104.1, 2008.
Nozawa, T., Nagashima, T., Yokohata, T., Okada, N., and Shiogama, H.: Climate Change Simulations with a Coupled Ocean-Atmosphere GCM Called the Model for Interdisciplinary Research on Climate?: MIROC Center for Global Environmental Research National Institute for Environmental Studies, Japan, 2007.
Ohgaito, R. and Abe-Ouchi, A.: The role of ocean thermodynamics and dynamics in Asian summer monsoon changes during the mid-Holocene, Clim. Dynam., 1, 39–50, doi:10.1007/s00382-006-0217-6, 2007.
Ohgaito, R. and Abe-Ouchi, A.: The effect of sea surface temperature bias in the PMIP2 AOGCMs on mid-Holocene Asian monsoon enhancement, Clim. Dynam., 33, 975–983, doi:10.1007/s00382-009-0533-8, 2009.
Oka, A., Hasumi, H., and Abe-Ouchi, A.: The thermal threshold of the Atlantic meridional overturning circulation and its control by wind stress forcing during glacial climate, Geophys. Res. Lett., 39, 1–6, doi:10.1029/2012GL051421, 2012.
Oki, T. and Sud, Y. C.: Design of Total Runoff Integrating Pathways (TRIP)–A Global River Channel Network, Earth Interactions, 2, 1–36, doi:10.1175/1087-3562(1998)002<0001:DoTRIP>2.0.CO;2, 1998.
Oschlies, A.: Model-derived estimates of new production: New results point towards lower values, Deep-Sea Res. II, 48, 2173– 2197, 2001.
Oschlies, A. and Garçon, V.: An eddy-permitting coupled physical-biological model of the North Atlantic 1. Sensitivity to advection numerics and mixed layer physics, Global Biogeochem. Cy., 13, 135–160, 1999.
Otto-Bliesner, B. L., Joussaume, S., Harrison, S. P., Abe-Ouchi, A., and Braconnot, P.: PMIP2 Workshop, PAGES news, 17, 42–43, 2009.

GMDD
5, 2527–2569, 2012



Paleoclimate Modelling Intercomparison Project Phase III: Ice Sheet for PMIP3/CMIP5 simulations, available at: https://pmip3.lsce.ipsl.fr/wiki/doku.php/pmip3:design:pi:final:icesheet, (last access: 28 August 2012), 2010.

Peltier, W. R. and Drummond, R.: Rheological stratification of the lithosphere: A direct inference based upon the geodetically observed pattern of the glacial isostatic adjustment of the North American, Geophys. Res. Lett., 35, 1–5, doi:10.1029/2008GL034586, 2008.

Peltier, W. R., Argus, D. F., Drummond, R., Gyllencreutz, R., Mangerud, J., Swensen, J.-I., and Lohne, O. S.: Space Geodesy Constrains Ice-Age Terminal Deglaciation, Nature, submitted, 2012.

Peyron, O., Jolly, D., Braconnot, P., Bonnefille, R., Guiot, J., Wirrmann, D. and Chalié, F.: Quantitative reconstructions of annual rainfall in Africa 6000 years ago: Model-data comparison, J. Geophys. Res., 111, D24110, doi:10.1029/2006JD007396, 2006.

Pickett, E. J., Harrison, S. P., Hope, G., Harle, K., Dodson, J. R., Kershaw, A. P., Prentice, I. C., Backhouse, J., Colhoun, E. A., D'costa, D., Flenley, J., Grindrod, J., Haberle, S., Hassell, C., Kenyon, C., Macphail, M., Martin, H., Martin, A. H., Mckenzie, M., Newsome, J. C., Penny, D., Powell, J., Raine, J. I., Southern, W., Stevenson, J., Sutra, J. P., Thomas, I., Van Der Kaars, S., and Ward, J.: Pollen-based reconstructions of biome distributions for Australia, Southeast Asia and the Pacific (SEAPAC region) at 0, 6000 and 18 000 14C yr BP, J. Biogeogr., 31, 1381–1444, doi:10.1111/j.1365-2699.2004.01001.x, 2004.

Pinto, J. P., Turco, R. P., and Toon, O. B.: Self-limiting Physical and Chemical Effects in Volcanic Eruption Clouds, J. Geophys. Res., 94, 11165–11174, doi:10.1029/JD094iD08p11165, 1989.

Plattner, B. G., Joos, F., Stocker, T. F., and Marchal, O.: Feedback mechanisms and sensitivities of ocean carbon uptake under global warming, Tellus, 53, 564–592, 2001a.

Plattner, B. G., Joos, F., Stocker, T. F., and Marchal, O.: Feedback mechanisms and sensitivities of ocean carbon uptake under global warming, Tellus, 53, 564–592, 2001b.

Prentice, I. C. and Jolly, D.: Mid-Holocene and glacial-maximum vegetation geography of the northern continents and Africa, J. Biogeogr., 27, 507–519, doi:10.1046/j.1365-2699.2000.00425.x, 2000.

Ray, N. and Adams, J. M.: A GIS-based Vegetation Map of the World at the Last Glacial Maximum (25 000-15 000 BP), Internet Archaeol., 11, 1–44, 2001.

GMDD

5, 2527–2569, 2012



Rojas, M., Moreno, P., Kageyama, M., Crucifix, M., Hewitt, C., Abe-Ouchi, A., Ohgaito, R., Brady, E. C., and Hope, P.: The Southern Westerlies during the last glacial maximum in PMIP2 simulations, Clim. Dynam., 32, 525–548, doi:10.1007/s00382-008-0421-7, 2008.

Sato, H., Itoh, A., and Kohyama, T.: SEIB–DGVM: A new Dynamic Global Vegetation Model using a spatially explicit individual-based approach, Ecol. Modell., 200, 279–307, doi:10.1016/j.ecolmodel.2006.09.006, 2007.

Sato, M., Hansen, J. E., Mccormick, M. P., and Pollack, J. B.: Stratospheric aerosol optical depths, 1850–1990, J. Geophys. Res.-Atmos., 98, 22987–22994, 1993.

Schmidt, G. A., Jungclaus, J. H., Ammann, C. M., Bard, E., Braconnot, P., Crowley, T. J., Delaygue, G., Joos, F., Krivova, N. A., Muscheler, R., Otto-Bliesner, B. L., Pongratz, J., Shindell, D. T., Solanki, S. K., Steinhilber, F., and Vieira, L. E. A.: Climate forcing reconstructions for use in PMIP simulations of the Last Millennium (v1.1), Geosci. Model Dev., 5, 185–191, doi:10.5194/gmd-5-185-2012, 2012.

Schmittner, A., Urban, N. M., Shakun, J. D., Mahowald, N. M., Clark, P. U., Bartlein, P. J., Mix, A. C., and Rosell-Mele, A.: Climate Sensitivity Estimated from Temperature Reconstructions of the Last Glacial Maximum, Science, 334, 1385–1388, doi:10.1126/science.1203513, 2011.

Semtner, A. J.: A Model for the Thermodynamic Growth of Sea Ice in Numerical Investigations of Climate, J. Phys. Oceanogr., 6, 379–389, doi:10.1175/1520-0485(1976)006<0379:AMFTTG>2.0.CO;2, 1976.

Servonnat, J., Yiou, P., Khodri, M., Swingedouw, D., and Denvil, S.: Influence of solar variability, CO_2 and orbital forcing between 1000 and 1850 AD in the IPSLCM4 model, Clim. Past, 6, 445–460, doi:10.5194/cp-6-445-2010, 2010.

Shindell, D. T., Schmidt, G. A., Mann, M. E., Rind, D.m and Waple, A.: Solar forcing of regional climate change during the Maunder Minimum, Science, 294, 2149–2152, doi:10.1126/science.1064363, 2001.

Takata, K., Emori, S., and Watanabe, T.: Development of the minimal advanced treatments of surface interaction and runoff, Global Planet. Change, 38, 209–222, doi:10.1016/S0921-8181(03)00030-4, 2003.

Takemura, T.: Simulation of climate response to aerosol direct and indirect effects with aerosol transport-radiation model, J. Geophys. Res., 110, D02202, doi:10.1029/2004JD005029, 2005.

GMDD
5, 2527–2569, 2012



Takemura, T., Okamoto, H., Maruyama, Y., Numaguti, A., Higurashi, A., and Nakajima, T.: Global three-dimensional simulation of aerosol optical thickness distribution of various origins, J. Geophys. Res., 105, 17853–17873, doi:10.1029/2000JD900265, 2000.
Takemura, T., Nakajima, T., Dubovik, O., Holben, B. N., and Kinne, S.: Single-Scattering Albedo and Radiative Forcing of Various Aerosol Species with a Global Three-Dimensional Model, J. Climate, 15, 333–352, doi:10.1175/1520-0442(2002)015<0333:SSAARF>2.0.CO;2, 2002.
Tans, P. and Keeling, R.: Trends in Atmospheric Carbon Dioxide, available at: http://www.esrl.noaa.gov/gmd/ccgg/trends/, last access: 30 March 2012.
Tarasov, L. and Peltier, W. R.: Greenland glacial history and local geodynamic consequences, Geophys. J. Int., 150, 198–229, doi:10.1046/j.1365-246X.2002.01702.x, 2002.
Tarasov, L. and Peltier, W. R.: Greenland glacial history, borehole constraints, and Eemian extent, J. Geophys. Res, 108, 1–20, doi:10.1029/2001JB001731, 2003.
Tarasov, P. E., Volkova, V. S., Webb, T., Guiot, J., Andreev, A. A., Bezusko, L. G., Bezusko, T. V., Bykova, G. V., Dorofeyuk, N. I., Kvavadze, E. V., Osipova, I. M., Panova, N. K. and Sevastyanov, D. V.: Last glacial maximum biomes reconstructed from pollen and plant macrofossil data from northern Eurasia, J. Biogeogr., 27(3), 609–620, doi:10.1046/j.1365-2699.2000.00429.x, 2000.
Taylor, K. E., Stouffer, R. J., and Meehl, G. A.: A summary of the CMIP5 experimental design, 2009, retrieved on: 26 June 2011, available at: http://cmip-pcmdi.llnl.gov/cmip5/docs/Taylor_CMIP5_design.pdf, 2011.
Taylor, K. E., Stouffer, R. J., and Meehl, G. A.: An Overview of CMIP5 and the Experiment Design, B. Am. Meteorol. Soc., 93, 485–498, doi:10.1175/BAMS-D-11-00094.1, 2012.
Trouet, V., Esper, J., Graham, N. E., Baker, A., Scourse, J. D., and Frank, D. C.: Persistent positive North Atlantic Oscillation mode dominated the medieval climate anomaly, Science, 324, p. 78, 2009.
Wang, Y.-M., Lean, J. L., and Sheeley, Jr. N. R.: Modeling the Sun's Magnetic Field and Irradiance since 1713, Astrophys. J., 625, 522–538, doi:10.1086/429689, 2005.
Watanabe, S., Miura, H., and Sekiguchi, M.: Development of an atmospheric general circulation model for integrated Earth system modeling on the Earth Simulator, J. Earth Simulator, 9, 27–35, 2008.
Watanabe, S., Hajima, T., Sudo, K., Nagashima, T., Takemura, T., Okajima, H., Nozawa, T., Kawase, H., Abe, M., Yokohata, T., Ise, T., Sato, H., Kato, E., Takata, K., Emori, S., and

GMDD
5, 2527–2569, 2012



Kawamiya, M.: MIROC-ESM 2010: model description and basic results of CMIP5-20c3m experiments, Geosci. Model Dev., 4, 845–872, doi:10.5194/gmd-4-845-2011, 2011.
Weber, S. L., Drijfhout, S. S., Abe-Ouchi, A., Crucifix, M., Eby, M., Ganopolski, A., Murakami, S., Otto-Bliesner, B., and Peltier, W. R.: The modern and glacial overturning circulation in the Atlantic ocean in PMIP coupled model simulations, Clim. Past, 3, 51–64, doi:10.5194/cp-3-51-2007, 2007.
World Ocean Atlas: Tech. rep., National Oceanographic Data Center, Silver Spring, Maryland, available at: http://www.esrl.noaa.gov/psd/, Version 2, 1998.
Xie, P. and Arkin, P. A.: Analyses of global monthly precipitation using gauge observations, satellite estimates, and numerical model predictions, J. Climate, 9, 840–858, 1996.
Yang, Z.-L., Dickinson, R. E., Robock, A., and Vinnikov, K. Y.: Validation of the Snow Submodel of the Biosphere–Atmosphere Transfer Scheme with Russian Snow Cover and Meteorological Observational Data, J. Climate, 10, 353–373, doi:10.1175/1520-0442(1997)010<0353:VOTSSO>2.0.CO;2, 1997.
Yu, G., Chen, X., Ni, J., Cheddadi, R., Guiot, J., Han, H., Harrison, S. P., Huang, C., Ke, M., Kong, Z., Li, S., Li, W., Liew, P., Liu, G., Liu, J., Liu, Q., Liu, K. B., Prentice, I. C., Qui, W., Ren, G., Song, C., Sugita, S., Sun, X., Tang, L., Vancampo, E., Xia, Y., Xu, Q., Yan, S., Yang, X., Zhao, J., and Zheng, Z.: Palaeovegetation of China: a pollen data-based synthesis for the mid-Holocene and last glacial maximum, J. Biogeogr., 27, 635–664, doi:10.1046/j.1365-2699.2000.00431.x, 2000.
Zhao, Y. and Harrison, S. P.: Mid-Holocene monsoons: a multi-model analysis of the inter-hemispheric differences in the responses to orbital forcing and ocean feedbacks, Clim. Dynam., online first, doi:10.1007/s00382-011-1193-z, 2011.
Zhao, Y., Braconnot, P., Marti, O., Harrison, S. P., Hewitt, C., Kitoh, A., Liu, Z., Mikolajewicz, U., Otto-Bliesner, B., and Weber, S. L.: A multi-model analysis of the role of the ocean on the African and Indian monsoon during the mid-Holocene, Clim. Dynam., 25, 777–800, doi:10.1007/s00382-005-0075-7, 2005.
Zhao, Y., Braconnot, P., Harrison, S. P., Yiou, P., and Marti, O.: Simulated changes in the relationship between tropical ocean temperatures and the western African monsoon during the mid-Holocene, Clim. Dynam., 28, 533–551, doi:10.1007/s00382-006-0196-7, 2007.

GMDD
5, 2527–2569, 2012



Table 1. The boundary conditions for the each experiment.

abbr. name	PI	6 ka	LGM	LM
period	pre-industrial 1850 AD	mid-Holocene 6000 yr before present	Last Glacial Maximum 21 000 yr before present	Last Millennium 850–1850 AD
Experiment no. in CMIP5	Exp. 3.1	Exp. 3.4	Exp. 3.5	Exp. 3.6
Type	time slice	time slice	time slice	Transient
land boundary condition	pre-industrial	pre-industrial	LGM topography	pre-industrial
GHG : CO_2 (ppm)	285.0	280.0	185.0	Prognostic
GHG : N_2O (ppm)	0.31	0.27	0.20	given, time variable
GHG : CH_4 (ppm)	1.7414	0.65	0.35	given, time variable
orbit: eccentricity	0.01672	0.018682	0.018994	given, time variable
orbit: obliquity (°)	23.45	24.105	22.949	given, time variable
orbit: angular precession (°)	102.04	0.87	114.42	given, time variable

GMDD
5, 2527–2569, 2012



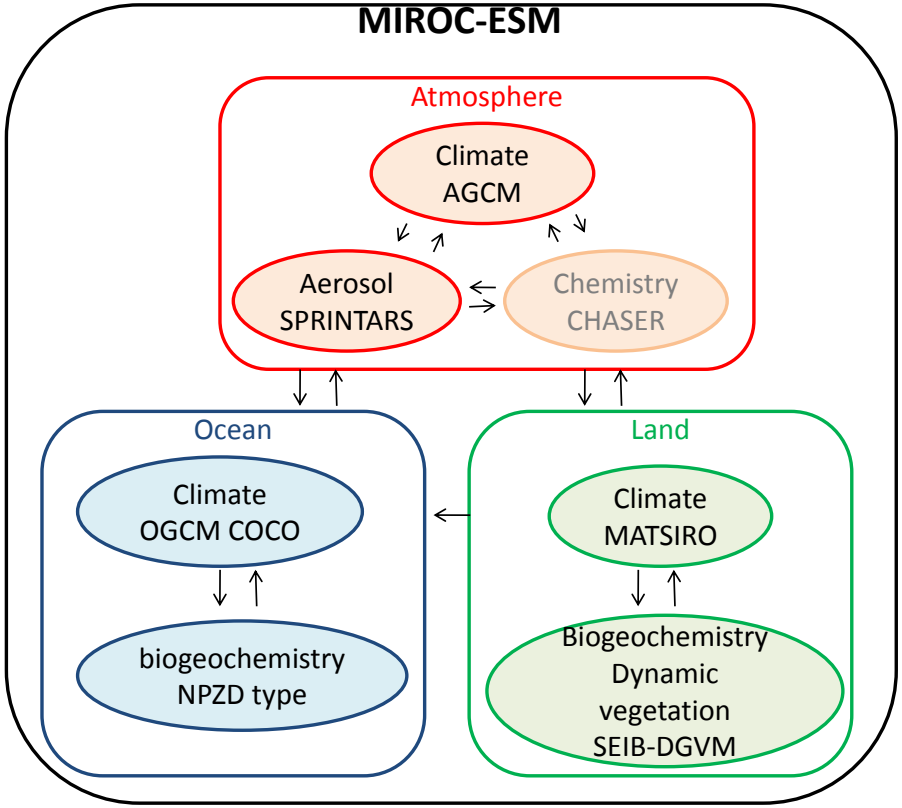


Fig. 1. The structure of MIROC-ESM.

GMDD
5, 2527–2569, 2012



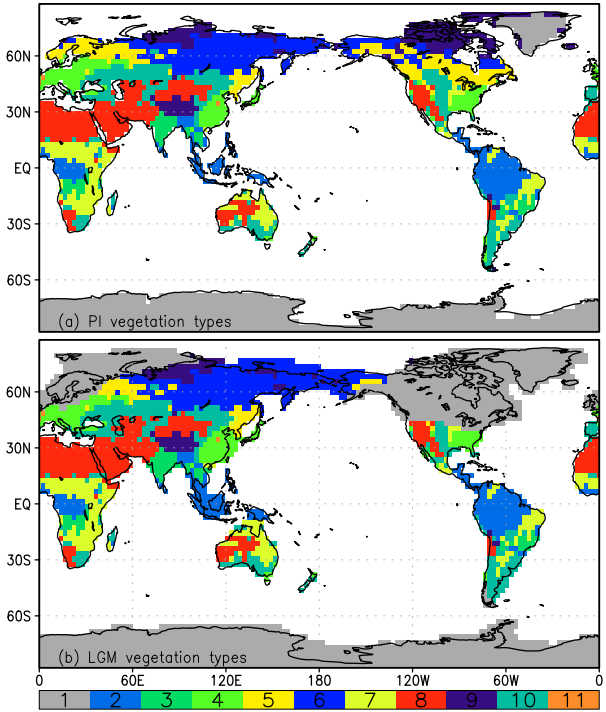


Fig. 2. The vegetation types for the land model MATSIRO for **(a)** PI and **(b)** LGM. #0 – sea surface, #1 – continental ice, #2 – broadleaf evergreen forest, #3 – broadleaf deciduous forest and woodland, #4 – mixed coniferous and broadleaf deciduous forest and woodland, #5 – coniferous forest and woodland, #6 – high latitude deciduous forest and woodland, #7 – wooded C4 grassland, #8 – shrubs and bare ground, #9 – tundra, #10 – C3 grassland, #11 – cultivation.

GMDD
5, 2527–2569, 2012



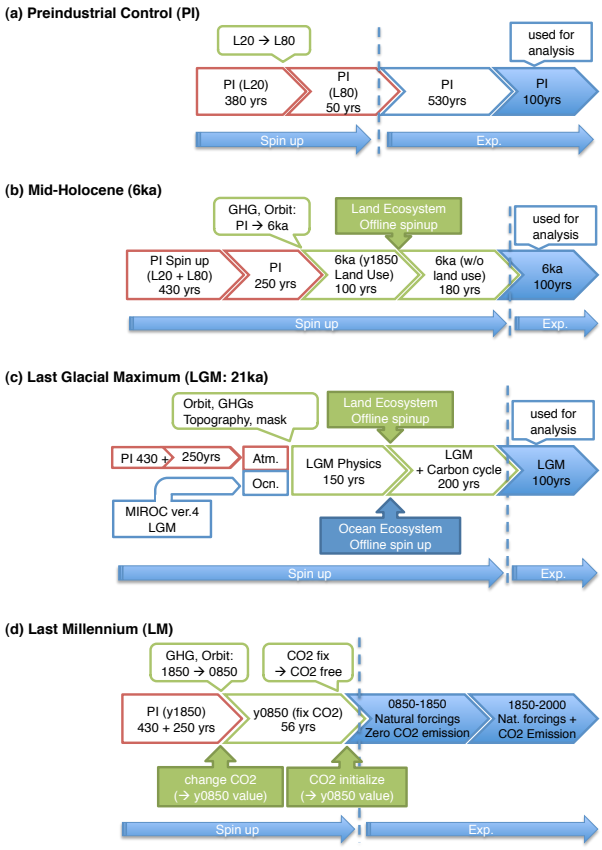


Fig. 3. The procedure of initial data preparation: **(a)** Pre-industrial control: PI, **(b)** Mid Holocene: 6 ka, **(c)** Last Glacial Maximum (LGM): 21 ka, **(d)** Last Millennium: LM.

GMDD
5, 2527–2569, 2012

Setup of the PMIP3 paleoclimate experiments using MIROC-ESM

T. Sueyoshi et al.



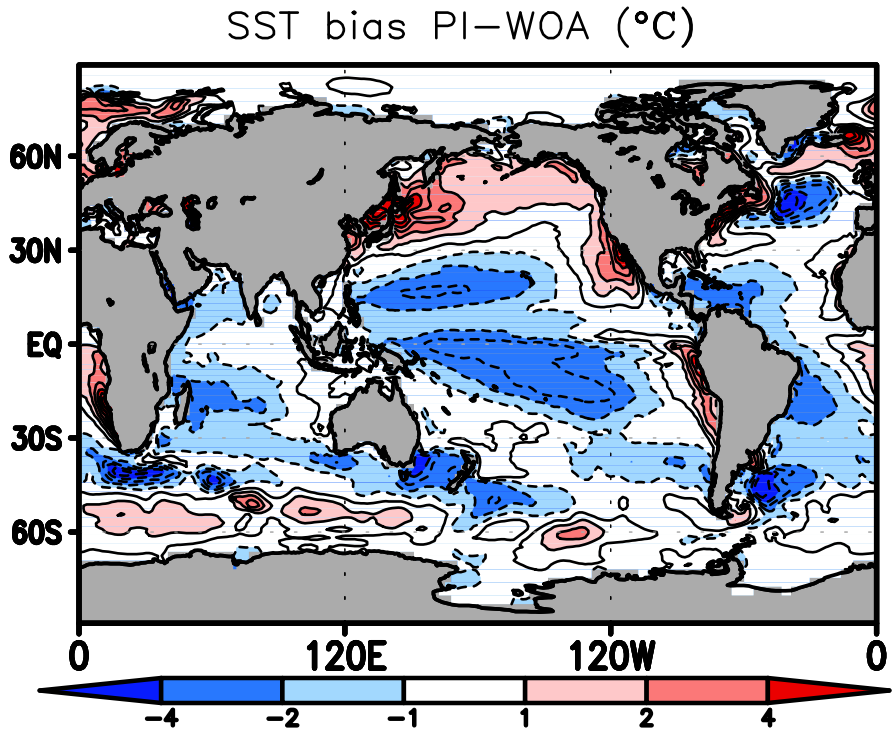


Fig. 4. The global annual mean sea surface temperature representation (˚C) of PI in comparison with World Ocean Atlas SST (WOA, 2009).

GMDD
5, 2527–2569, 2012



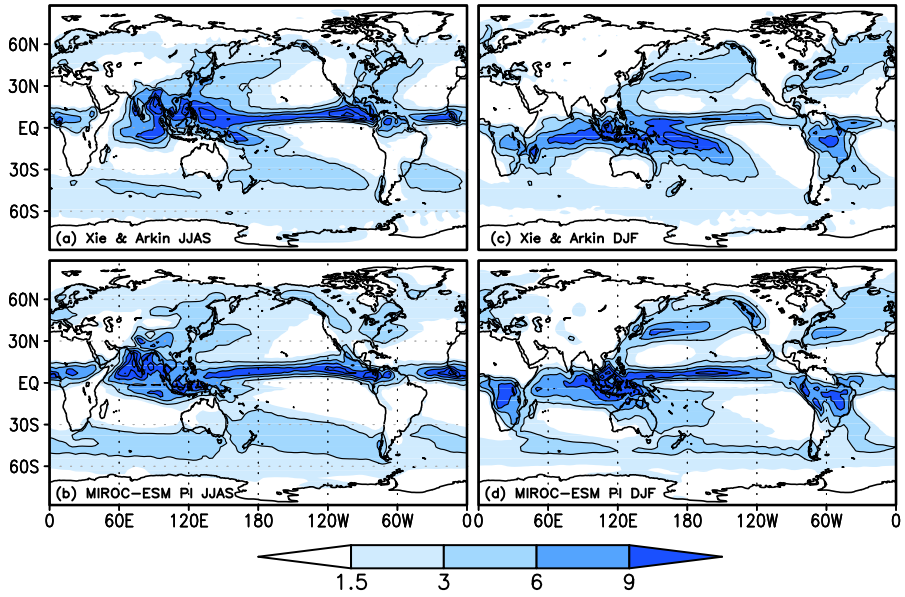


Fig. 5. The global precipitation distribution (mm day^{-1}) of PI for JJAS and DJF **(b, d)** in comparison with re-analysis data (Xie and Arkin, 1996) **(a, c)**.

GMDD
5, 2527–2569, 2012



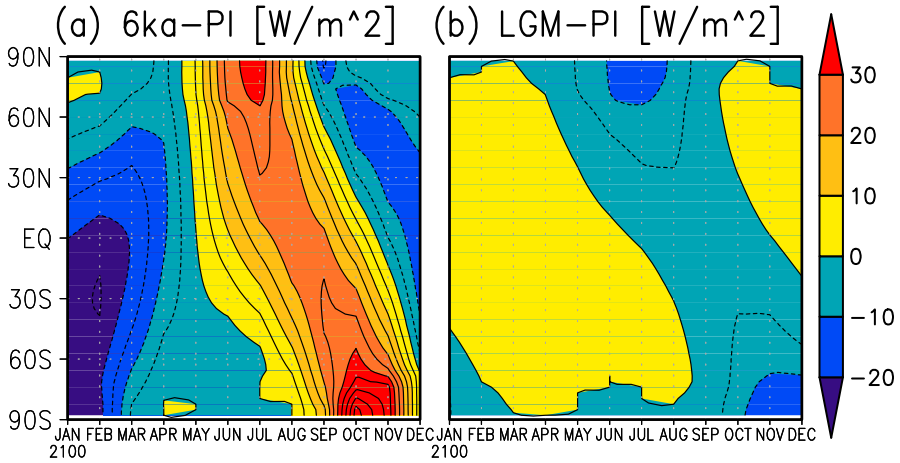


Fig. 6. The short wave radiation change ($W\,m^{-2}$) at the top of the atmosphere for 6 ka-PI, LGM-PI.

GMDD
5, 2527–2569, 2012



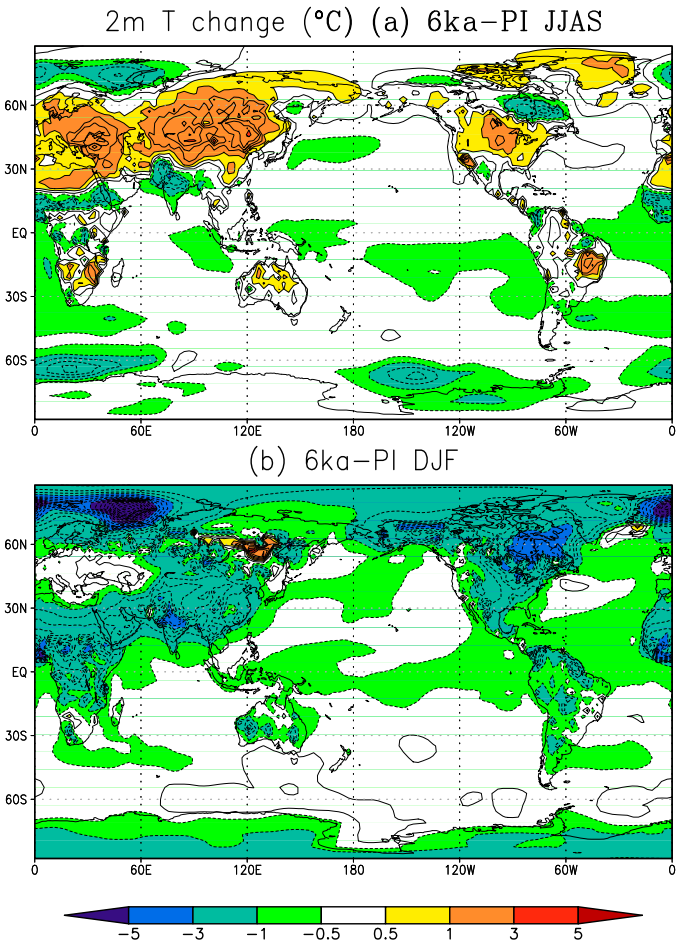


Fig. 7. The surface temperature change 6 ka-PI (˚C) for **(a)** JJAS and **(b)** DJF.

GMDD
5, 2527–2569, 2012



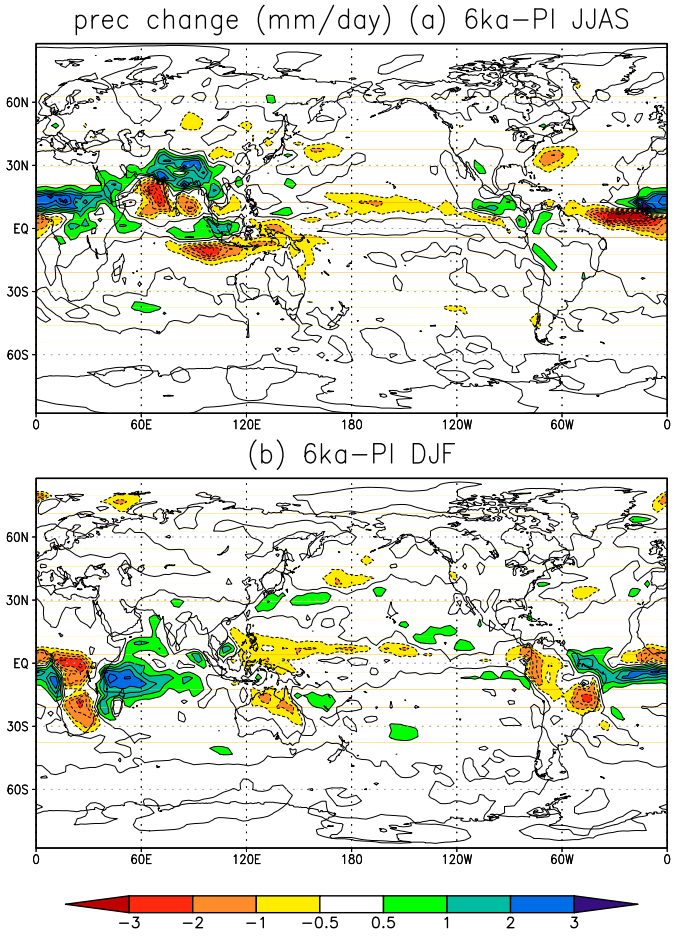


Fig. 8. The precipitation change 6 ka-PI (mm day^{-1}) for **(a)** JJAS and **(b)** DJF.

GMDD
5, 2527–2569, 2012

Setup of the PMIP3 paleoclimate experiments using MIROC-ESM

T. Sueyoshi et al.



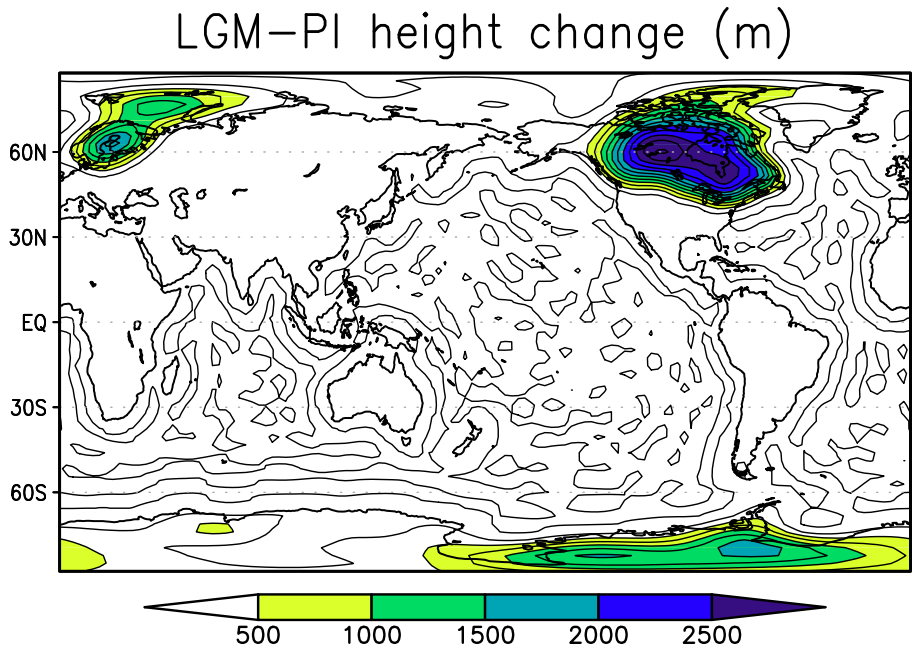


Fig. 9. The orographic change for LGM-PI (m).

GMDD
5, 2527–2569, 2012



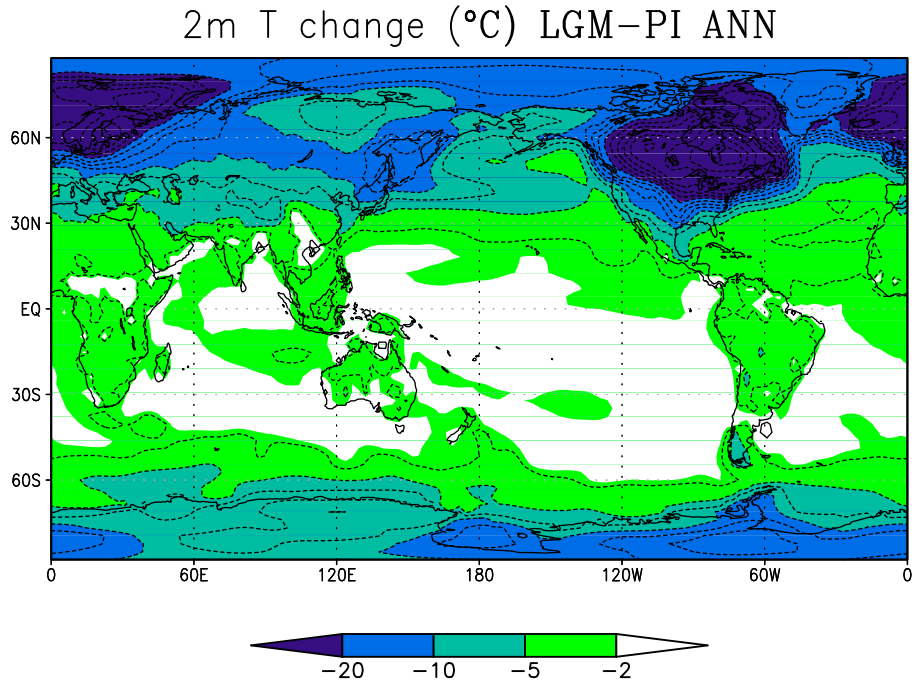


Fig. 10. The annual mean temperature change LGM-PI (°C).

GMDD
5, 2527–2569, 2012



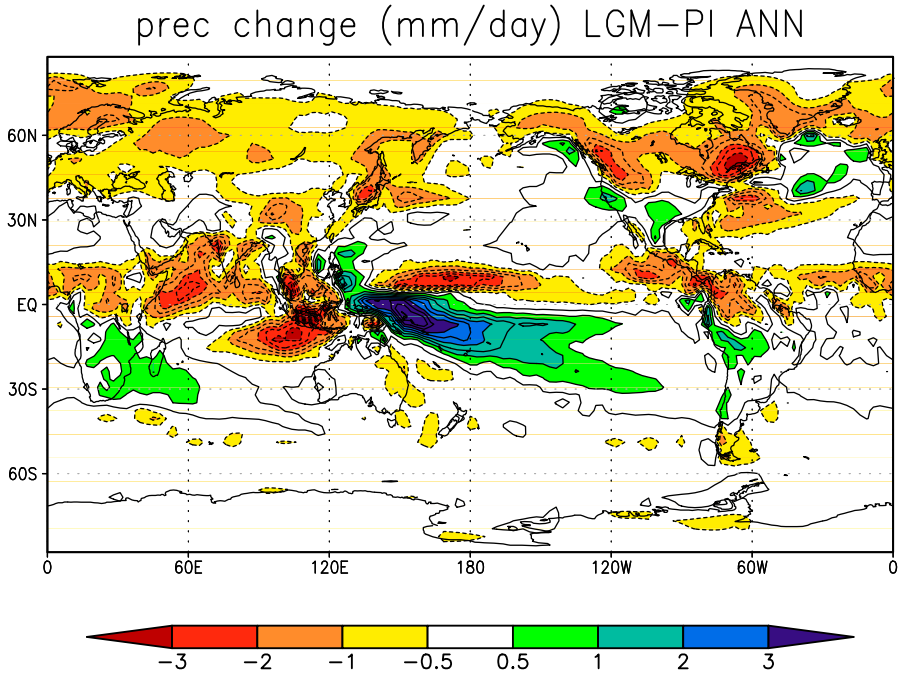


Fig. 11. The annual mean precipitation change LGM-PI (mm day^{-1}).

GMDD
5, 2527–2569, 2012



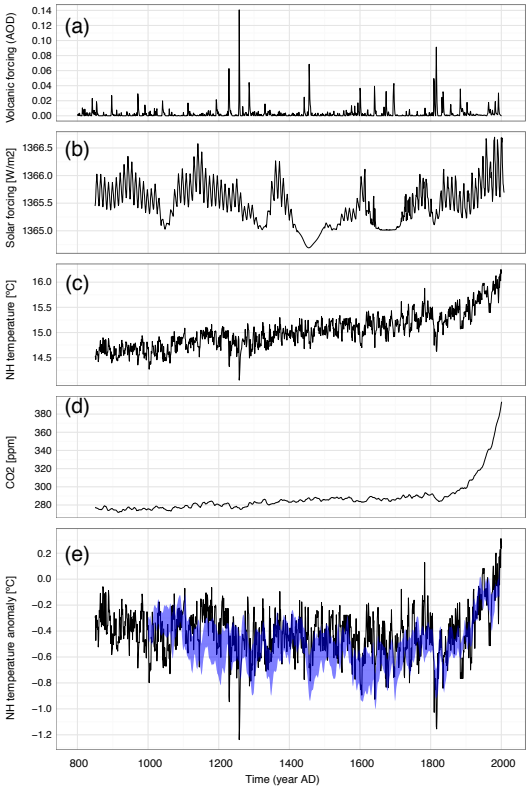


Fig. 12. The **(a)** solar and **(b)** volcanic forcing, **(c)** annual mean surface air temperature in the Northern Hemisphere, **(d)** model-predicted atmospheric CO_2 concentration, **(e)** detrended time series of mean annual surface air temperature anomaly (anomaly from the 1970–2000 mean). The blue shading represents the range of temperature reconstruction between the 20th and 80th percentile by Frank et al. (2010).

GMDD
5, 2527–2569, 2012

